Structural and chemical properties of the nitrogen-rich energetic material triaminoguanidinium 1-methyl-5-nitriminotetrazolate under pressure

R. Stewart McWilliams,[1,2] Yasmin Kadry,[1,2] Mohammad F. Mahmood,[1,2] Alexander F. Goncharov,[2] and Jennifer Ciezak-Jenkins[2,3]
[1]*Howard University, Washington, DC 20059, USA*
[2]*Geophysical Laboratory, Carnegie Institution of Washington, Washington, DC 20015, USA*
[3]*RDRL-WML-B, U.S. Army Research Laboratory, Aberdeen Proving Grounds, Maryland 21005, USA*

(Received 14 November 2011; accepted 15 June 2012; published online 1 August 2012)

The structural and chemical properties of the bi-molecular, hydrogen-bonded, nitrogen-rich energetic material triaminoguanidinium 1-methyl-5-nitriminotetrazolate $C_3H_{12}N_{12}O_2$ (TAG-MNT) have been investigated at room pressure and under high pressure isothermal compression using powder x-ray diffraction and Raman and infrared spectroscopy. A stiffening of the equation of state and concomitant structural relaxation between 6 and 14 GPa are found to correlate with Raman mode disappearances, frequency discontinuities, and changes in the pressure dependence of modes. These observations manifest the occurrence of a reversible martensitic structural transformation to a new crystalline phase. The onset and vanishing of Fermi resonance in the nitrimine group correlate with the stiffening of the equation of state and phase transition, suggesting a possible connection between these phenomena. Beyond 15 GPa, pressure induces irreversible chemical reactions, culminating in the formation of a polymeric phase by 60 GPa. © *2012 American Institute of Physics*. [http://dx.doi.org/10.1063/1.4732097]

I. INTRODUCTION

From fuels to explosives, energetic materials are crucially important for industrialized civilization, and in the search for new energetic materials with improved properties many radically different substances have been synthesized. Integration of these materials into practical applications—and the identification and engineering of further improvements—requires an understanding of the unique reaction pathways of these systems. Such studies are challenging, as reaction and decomposition mechanisms depend on environmental factors such as stress, temperature, and loading rate. High pressures, for example, are encountered in detonation reactions, yet persist for such a short time as to limit characterization of material state and chemical processes. Static compression studies, alternatively, can reveal basic details regarding molecular deformation, interaction, and decomposition under pressure using sensitive spectroscopic and structural measurements, forming a baseline for understanding chemistry under rapid application of stress (and temperature) as is found during detonation.[1]

There is considerable current interest in the design and synthesis of nitrogen-rich energetic materials.[2,3] Such materials have the potential for storage and liberation of energies comparable to or greater than conventional energetic materials with chemistries based solely on carbon-hydrogen-nitrogen-oxygen, due to the substantial energy difference between the N–N single bond (160 kJ/mol) and the N≡N triple bond (954 kJ/mol). Additionally, explosive formulations which utilize nitrogen-rich energetic materials pose significantly lower environmental and safety hazards than conventional energetic materials such as RDX (1,3,5-trinitro-1,3,5-triazacyclohexane), as these materials can have high thermal stabilities with a primary decomposition product of molecular nitrogen (N_2). Although energetic phases of pure nitrogen (i.e., nonmolecular or polymeric phases) have been synthesized under high temperature and pressure,[3–8] it has not been demonstrated that such all-nitrogen energetic materials can be used in practical applications.

Triaminoguanidinium 1-methyl-5-nitriminotetrazolate ($C_3H_{12}N_{12}O_2$), or TAG-MNT, is an energetic, nitrogen-rich "salt" first synthesized in 2008 which belongs to a large class of recently discovered nitrogen-rich energetic materials based on the tetrazole moiety.[9] Among this general family of materials, TAG-MNT is of particular interest due to its similarity to RDX in several energetic performance tests; although the calculated detonation parameters of RDX are higher, Koenen tests on TAG-MNT suggested superior explosive performance.[9] TAG-MNT consists of two molecular ions, a triaminoguanidinium (TAG) cation and a 1-methyl-5-nitriminotetrazole (MNT) anion (Fig. 1). With an elemental concentration of nitrogen near 70%, the synthesis and performance testing of TAG-MNT represents a critical step toward the realization and implementation of practical high-nitrogen content energetic materials. In addition, the large elemental percentage of hydrogen in TAG-MNT may offer a route to achieving both insensitivity and high detonation pressure.[10,11]

Here we report on observations of the chemical and structural state of TAG-MNT under isothermal compression in a diamond-anvil cell to pressures similar to those observed during detonation[9] (27.3 GPa) using synchrotron x-ray diffraction, infrared absorption (IR) spectroscopy, and Raman spectroscopy. We have observed a martensitic structural transformation in TAG-MNT occurring between 9 and 13 GPa, followed by permanent pressure-induced chemical alteration above ∼20 GPa that ultimately leads to the synthesis of a polymeric phase. Shear stresses, which can

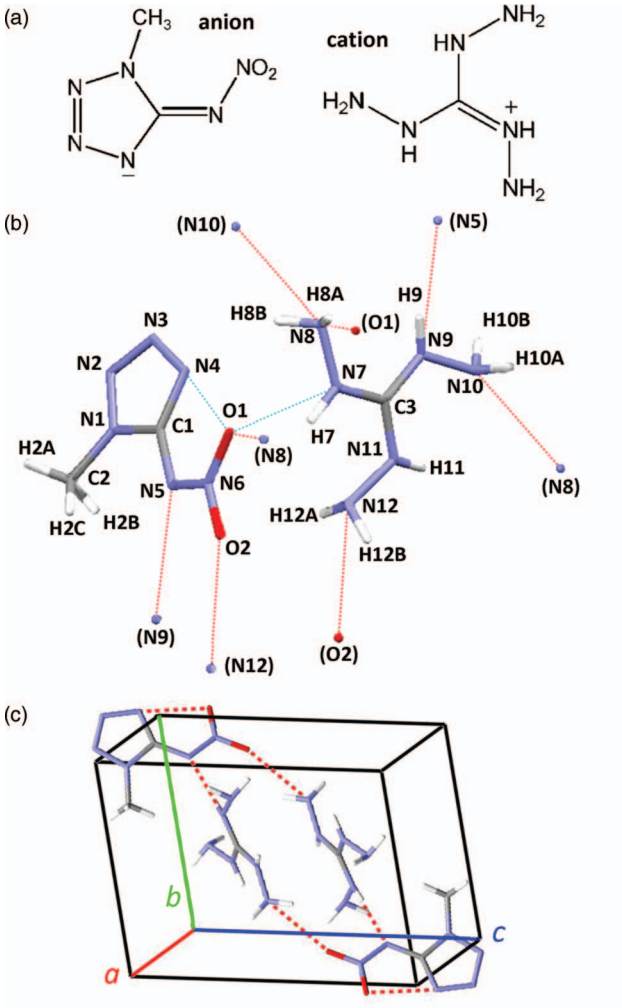

FIG. 1. Chemical and structural properties of TAG-MNT at ambient conditions.[9] (a) Triaminoguanidinium and 1-methyl-5-nitriminotetrazole molecular ions; the anion is deprotonated (leaving the lowermost ring nitrogen with negative charge) in salt form. (b) Molecular conformities, with hydrogen bonds shown as dotted lines and atoms in adjacent molecules labeled in parenthesis. (c) The triclinic unit cell of TAG-MNT with dotted lines showing hydrogen bonds.

influence compression and decomposition behavior of energetic materials,[12,13] are found to have a noticeable effect on molecular vibration energies. The strengthening of the hydrogen bond network in TAG-MNT under pressure evidently influences the response of this complex material to compression, activating Fermi resonances which may play a critical role in the compression response, and ultimately accommodating polymerization.

II. EXPERIMENTAL METHODS AND ANALYSIS

Polycrystalline TAG-MNT was synthesized and obtained from the Army Research Development and Engineering Center (ARDEC, Picatinny Arsenal, NJ) and used without further purification. The structural and spectroscopic properties of TAG-MNT were examined at ambient conditions and upon isothermal compression and decompression at room temperature using a diamond-anvil cell. Raman spectra at ambient conditions were collected from single crystal TAG-MNT, or on polycrystalline material recovered from high pressure. The pressure was monitored *in situ* during the experimental measurements using the ruby fluorescence method, which correlates the shifts of the R_1 and R_2 fluorescence lines of ruby to a well-defined equation of state[14] and, in some x-ray diffraction experiments, by the positions of diffraction peaks of solid neon. Samples were mechanically crushed into a fine polycrystalline powder and loaded into the diamond anvil cell (rhenium gasket) in a neon pressure medium (hydrostatic load) or as pure TAG-MNT without a medium (nonhydrostatic load), as is shown in Fig. 2. Ruby fluorescence measurements were typically made immediately preceding and after the x-ray diffraction and spectroscopy measurements to examine pressure drift during data collection. In the nonhydrostatic loadings, spectroscopic data were collected in close proximity to a ruby to minimize systematic errors in the pressure due to pressure gradients.

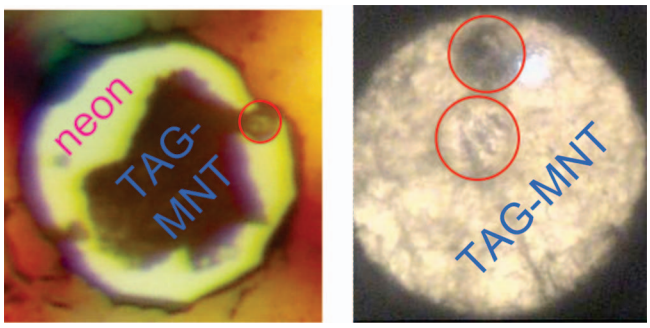

FIG. 2. Diamond-anvil cell samples of TAG-MNT in transmitted light, showing a powder loaded with a neon medium (left) and TAG-MNT loaded without a medium (right). Red circles indicate location of rubies used to measure pressure.

Raman spectra were collected using a confocal Raman microscope described previously.[15] The 488 nm line of either an argon ion or diode-pumped solid state laser was used as the principal excitation source, with a minimal laser power so as to prevent photochemical reactions in TAG-MNT over the 10–30 min acquisition time. In some cases, either the 457 nm line of a diode-pumped solid state laser, or the 632 nm line of a helium-neon laser was used. The spectrograph was a Jobin-Yvon HR460 employing a Princeton Instruments liquid-nitrogen cooled CCD. The Raman frequencies were extracted from the spectra using peak-fitting software developed in Igor Pro. The minimum measurable Raman shift was $\sim$80 cm^{-1}; measurement precision of $\sim$2.5 cm^{-1} was typical.

Synchrotron IR-absorption experiments were performed at beamline U2A of the National Synchrotron Light Source (NSLS) of Brookhaven National Laboratory (BNL). The synchrotron light is extracted from the VUV storage ring in a 40 $\times$ 40 mrad solid angle and the collimated beam is delivered through a vacuum pipe system and directed into a Bruker IFS 66v Fourier transform infrared (FTIR) spectrometer. Extensive detail of the optical layout of this beamline is available.[16] Infrared absorption spectra were collected between 600 and 4000 cm^{-1} with a spectral resolution of 2 cm^{-1}, over an average collection time of 12 min. Frequencies were extracted by peak fitting.

Powder angle-dispersive x-ray diffraction experiments were conducted at the ID-D beamline of GeoSoilEnviroCARS (GSECARS), Sector 13, Advanced Photon Source (APS), Argonne National Laboratory.[17] The x-ray wavelength

was 0.3344 Å. Cubic BN seats permitted measurement to large 2θ ($\sim 25^\circ$). For the x-ray diffraction patterns collected at ambient pressure, polycrystalline TAG-MNT was loaded into a diamond anvil cell but no stress was placed on the sample; for high pressures, a neon pressure medium was loaded into the cell to ensure hydrostatic stress. Generally, the x-ray diffraction patterns were found to be strongly sensitive to nonhydrostatic stresses, which arose either in loads of pure TAG-MNT, or in neon loads at high pressure where the sample cavity closed down on the powder. Attempts were made to limit the x-ray damage to the samples by strongly attenuating the x-ray beam and rastering the beam over the TAG-MNT samples. Each raster position corresponded to collection of a single x-ray pattern for ~ 20 s, with ~ 100 patterns collected per pressure point. The rastered patterns were integrated and reduced using the software Fit2D.[18] Background, defined by a cubic-spline interpolation between selected minima in the diffraction patterns, was subtracted.

Structural parameters were determined from the diffraction patterns through a combination of peak fitting, unit cell refinement using the software UnitCell, and pattern prediction and le Bail fitting using the software Powdercell 2.4. Unit cell parameters at pressure were initially estimated from lower pressure values and pressure derivatives. Observed patterns were compared with predicted patterns (assuming fractional atomic positions in the unit cell were constant under compression), and unit cell parameters were refined based on the most prominent and clearly identifiable diffraction peaks (typically, about 10 were used). The quality of the refinement was assessed by the precision of least-squares fitting in UnitCell and by finding the best overall congruence between the shapes of the predicted and observed diffraction patterns. With increasing pressure, there was an increasing deviation between observed and predicted peak intensities, indicating that the assumption of fixed fractional atomic positions imposed unphysical changes in interatomic distances during refinement. However, the general shape of the predicted and observed diffraction patterns, including the positions of prominent peaks, agreed well to high pressures, and even small perturbations from ideal unit cell parameters lead to a dramatic breakdown of pattern congruence. Unit cell parameters were finally refined using le Bail fitting, excluding signals from Ne and Re. While le Bail fitting substantially improved the agreement between the predicted and observed patterns at high pressure, the changes in unit cell parameters were statistically insignificant. Refinement of atomic positions within the unit cell was not attempted, due to the 29 atom basis, the low symmetry of the lattice (triclinic) and molecules (C_1), the need to account for molecular structure constraints (i.e., to locate hydrogen atoms) using, for example, density functional theory (DFT),[19] and the difficulty in measuring peak location and intensity for weak or overlapping reflections.

Volume data were analyzed using up to a fourth-order Birch-Murnaghan (BM) equation of state[20]

$$P(f) = 3K_0 f(1+2f)^{5/2}\left[1+\frac{3}{2}(K^{/}-4)f + \frac{3}{2}\left(K_0K^{//}+K^{/}(K^{/}-7)+\frac{143}{9}\right)f^2\right], \quad (1)$$

where $f = (1/2)[(V_0/V)^{2/3} - 1]$, V_0 is the initial volume, V is the volume under pressure, K_0 is the ambient bulk modulus, and $K^{/}$ and $K^{//}$ are the first and second pressure derivatives of the bulk modulus at ambient conditions, respectively. Equation (1) becomes the third-order BM equation if the third term in brackets is eliminated.

III. COMPUTATIONAL METHODS

To characterize the vibrational properties of TAG-MNT, DFT calculations were performed with the GUASSIAN Suite program package[21] using the B3LYP density functional[22–24] and the 6-31G** basis set located on the U.S. Army Research Laboratory DoD Supercomputing Resource Center. Isolated molecules of TAG and MNT were optimized using the tight convergence criteria and the vibrational frequencies were calculated from the Hessian matrix. The resulting vibrational frequencies were scaled by 0.961 in accordance with conventional DFT practices.[25]

IV. RESULTS

A. Properties at ambient pressure

At ambient conditions, the observed powder x-ray diffraction pattern for TAG-MNT is similar to that expected based on the previously reported structure.[9] Small refinements of the unit cell (Table I), based on the best-resolved peaks at $2\theta < 5^\circ$ in the powder pattern, bring the predicted pattern into excellent agreement with the data to $2\theta > 13^\circ$ (Fig. 3). The refined unit cell volume was slightly larger than that reported at lower temperature,[9] which we attribute to thermal expansion. The thermal expansivity of TAG-MNT thus inferred (Table I) is similar to RDX at comparable conditions.[26]

The Raman spectrum of TAG-MNT collected in this study at ambient conditions is similar to that reported previously,[9] though we observe considerable complexity in the spectrum that was not previously described (Fig. 4,

TABLE I. Structural and thermodynamic properties of TAG-MNT at ambient pressure; ρ is the density; K_T is the isothermal bulk modulus (obtained from fitting equation of state data to 6 GPa with a third-order Birch-Murnaghan equation); T is the temperature; α_V is the volumetric thermal expansion estimated from the volume difference between the 200 and 293 K data. Uncertainties in the present structural parameters are based on refinement precision reported by UnitCell and were confirmed by le Bail fitting.

	Klapötke *et al.*	This study
a (Å)	6.8650(2)	6.911(6)
b (Å)	7.9800(2)	8.005(9)
c (Å)	10.5180(3)	10.55(2)
α (°)	101.311(2)	101.0(1)
β (°)	103.776(2)	103.4(1)
γ (°)	103.123(2)	103.67(7)
V (Å)^3	525.60(3)	533(1)
ρ (g/cm^3)	1.569	1.547(3)
K_T (GPa)		14.6(9)
T (K)	200	293.3(1)
α_V (10^4/K)		1.5(2)

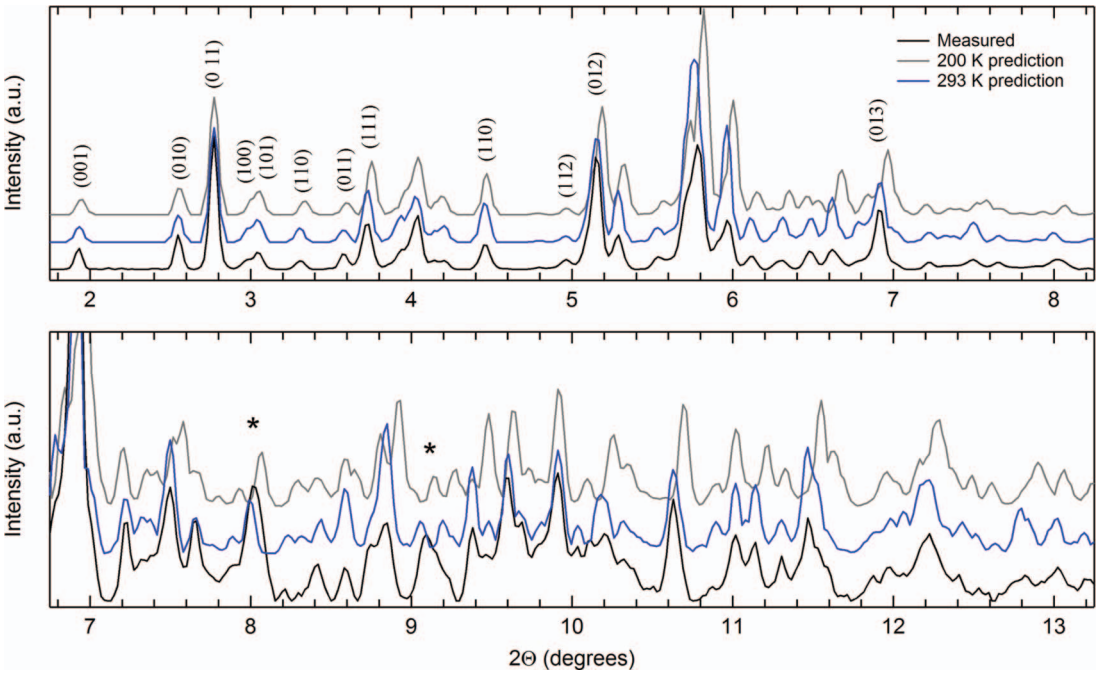

FIG. 3. X-ray diffraction data at ambient pressure and temperature (black), and pattern predictions based upon the previous crystallographic determination at 200 K (grey) (Ref. 9) and refined (blue) structures for room temperature (293 K). Prominent peaks are labeled with reciprocal lattice planes. Small contributions from the Rhenium gasket are identified with a star. Le Bail fitting improvements not included.

Table II). Many weak and asymmetric peaks are discerned (Fig. 4) and noted to split into multiple features upon compression (Fig. 5). The vibrational frequencies of the features observed in the infrared spectrum, which were extrapolated to ambient pressure, show generally good agreement with the previously reported lines, though several previously unreported features are identified (Fig. 5, Table II).

With 29 atoms in two molecular ions (each with C_1 molecular symmetry), 81 unique internal molecular modes of vibration can be expected for TAG-MNT at ambient conditions. Approximately 70 spectral features were observed in this study. Table II presents a summary of observed spectral lines, and compares line positions to those reported previously.[9] Additionally, Table II provides assignments of the molecular motions associated with the vibrational features based on our DFT calculations.

Strong IR- and Raman-active spectral lines near 1510 and 1550 cm^{-1} are of particular interest for this study. The former was identified as the "most significant" peak in the Raman spectrum of these salts and assigned to the anionic C=N stretch mode (ν C=N),[9] whereas the latter might be associated with the asymmetric stretch mode of the anion NO_2 group (ν_{as} NO_2) which was calculated to occur at similar frequencies.[9] However, our DFT predictions showed that the 1510 and 1550 cm^{-1} lines are more likely associated with ν_{as} NO_2 and ν C=N, respectively. Our assignment remains consistent with the previously calculated frequencies of these modes in the anion alone (1480–1560 cm^{-1}),[9]

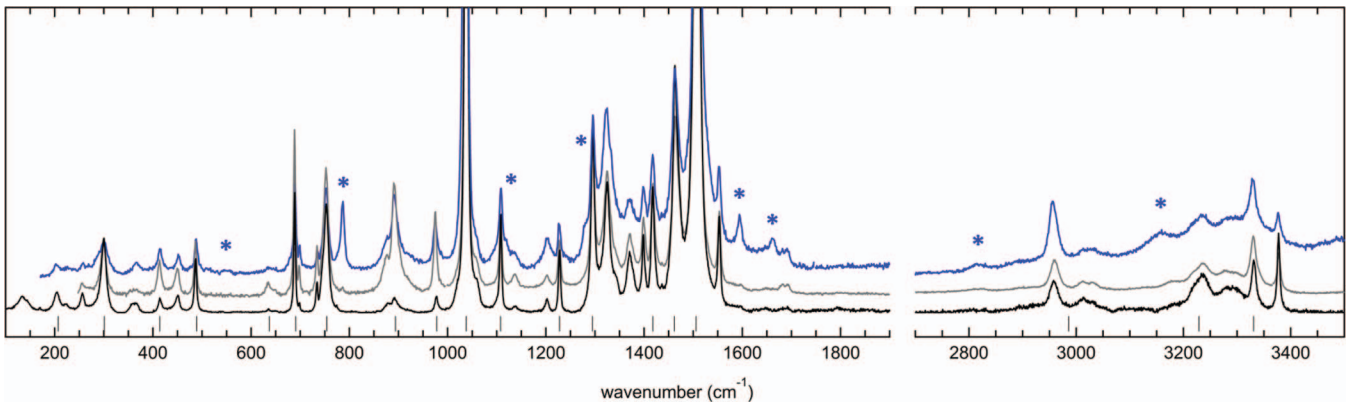

FIG. 4. Raman spectra of TAG-MNT at ambient pressure, for pristine material and previously compressed material. The black spectrum was obtained using an uncompressed single crystal; the grey (blue) spectra were obtained from a polycrystalline sample nonhydrostatically compressed to 15.6 ± 0.1 GPa (26 ± 1 GPa) and then decompressed; 488 nm (black) and 457 nm (grey, blue) excitation was used. Previously reported Raman lines[9] are black vertical lines near the bottom axis. Spectral features appearing as a result of pressure-induced chemistry are marked with a star.

TABLE II. Frequencies (in cm^{-1}) of observed Raman and IR lines in the present study at ambient pressure and 0.6 GPa, respectively, compared with previously observed spectral lines at zero pressure.[9] Predicted vibrational mode frequencies, and corresponding mode assignments, are based on DFT calculations as described in the text. The assigned modes in most cases consist of vibrations in a number of bonds; these are listed with the strongest contribution to the mode's properties appearing first.

This work, experiment		Klapötke *et al.*[9]		This work, calculation		
Raman 0 GPa	Infrared 0.6 GPa	Raman 0 GPa	Infrared 0 GPa	B3LYP 6-31G** (Ref. 25)	Assign.	Molecular motion
				25	an.	τ NO_2
		207		41, 173	an.	τ CH_3
257				110, 165, 267	an.	τ Skeletal
				115, 166	cat.	τ NH_2
				237, 403	cat.	τ Skeletal
300, 362		301		320, 321, 388	cat.	τ NH_2
				323	an.	τ CH_3, δ C–N–N
415		414		427	an.	ν C–N, τ Skeletal
450				463	an.	ω NO_2, ν C–N, ν N–N, ν N–CH_3
487		489				Overtone/combination
635	607	637		553, 622, 623	cat.	ω N–H, ω NH_2
649	642			627,628	cat.	δ N–C–N, δ C–N–N
	662			668	an.	δ N–N–C, δ N=N–N
689	688	691		678	an.	ν N–CH_3, ω NO_2
698	701		687	698	cat.	δ N–C–N, ω NH_2
				714	an.	ω N=C
734, 744, 753	736, 756	754	739	731, 757	an.	NO_2 umbrella, ν N–C–N, ν N–N, δ NO_2
	775, 796, 821		773			Overtones/combination
	848			852	an.	ν N–C–N, ν C=N, ν N–CH_3
877				872	cat.	ν C–N, ρ NH_2
892	889, 931	894	880	896, 910, 911	cat.	ν N–N, ρ NH_2
977		978		942	an.	δ N–N–C, ω CH_3
	989		979			Overtone/combination
1020, 1039	1015, 1039	1038	1036	1012, 1023	an.	Ring breathing, ν N–N, ν NO_2, ω C–H
1061				1092	an.	ν N–N, ω C–H, ν NO_2
1108	1110	1108	1107	1112	an.	ν N–N, ω N–H, ω NH_2
1140	1136		1132	1121, 1122, 1177	cat.	ν N–N, ω N–H, ω NH_2
1202	1201		1194	1199	an.	δ Ring
1228	1232	1228	1228	1204	an.	ν N=N, δ C=N–N, δ N–CH_3
				1275, 1277, 1278	cat.	ρ NH_2
1296	1293	1295		1294	an.	ν NO_2, ν N=N, δ N–CH_3
	1307			1319	an.	ν NO_2, ν N=N
1324, 1346	1331		1340	1331, 1332	cat.	δ C–N–N, ω N–H
1370						Overtones/combination
1376, 1399	1363, 1396			1377, 1394	an.	δ N–C–H, ν C–N
1418	1421	1418		1442	cat.	δ C–N–N, ω N–H
1436, 1462, 1466	1457	1462	1455	1448, 1454, 1492	an.	δ N–C–H, ν C–N
1507	1513	1506	1507	1494	an.	ν NO_2, ν C=N, ν C–N, ω C–H
1553	1550			1560	an.	ν C=N
1596, 1643	1596, 1648		1618	1590, 1638	cat.	δ C=N–N, δ NH_2
1687	1684		1676	1680, 1681	cat.	δ NH_2, ν C–N, δ C–N–H
1796, 1855						Overtones/combination
2344						N_2 impurity
2802, 2830, 2896, 2923						Overtones/combination
2959, 3012, 3032, 3092	3029	2986		2918, 2973, 3038	an.	ν C–H
3129, 3185, 3219, 3237, 3278, 3299, 3332, 3377	3129, 3173, 3209, 3378, 3325	3229, 3331	3207, 3322, 3371, 3469	3355, 3356, 3357, 3396, 3400, 3406, 3444, 3445, 3446	cat.	ν N–H

τ, Torsional; δ, bending; ρ, rocking; ω, wagging; ν, stretch; cat., cation; an., anion.

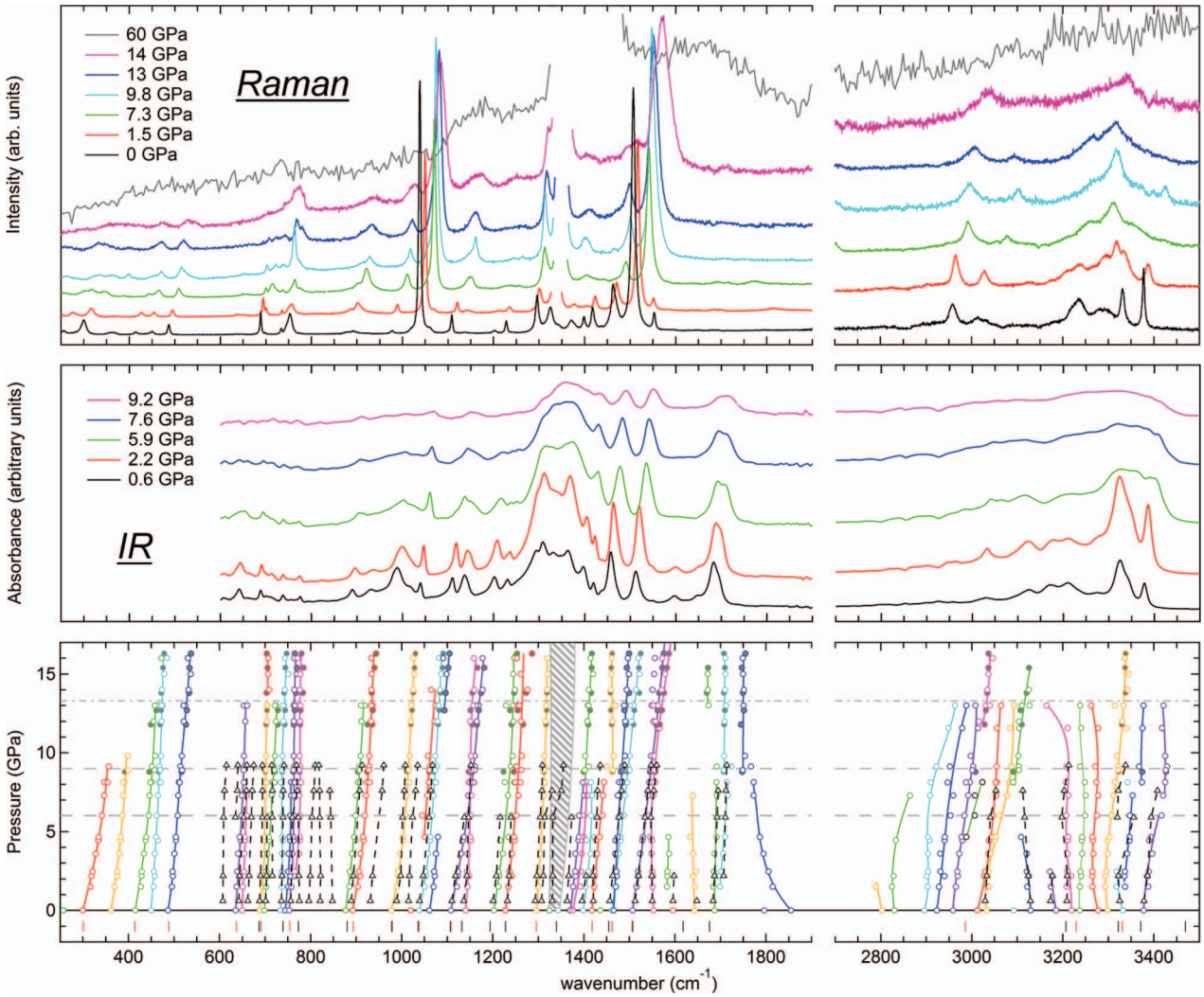

FIG. 5. Raman spectra (top), IR spectra (middle), and lineshifts with pressure (bottom). In the bottom panel, vertical red (black) dashes below 0 GPa (horizontal black line) are ambient Raman (IR) vibrational frequencies given by Klapötke *et al.*;[9] colored open (filled) circles represent Raman data from nonhydrostatic (hydrostatic) sample loadings; colored solid lines are second- to fifth-order polynomial fits to Raman lineshift data, pinned (when possible) at the ambient Raman frequency; grey hatched region represents the Raman signal of the diamond anvils; black triangles connected by dashed black lines are IR lineshift data; horizontal dashed grey lines represent the stiffening regime; horizontal dash-dotted grey line indicates the end of the high pressure structural transition. Raman peaks could be tracked with pressure reliably above 300 cm^{-1}; data shown here were collected using 488 or 457 nm excitation.

though some reduction in these frequencies (of ~50 cm^{-1}) is experimentally evident when the anion is placed in salt.[9] This assignment is consistent with the identification of the strong line at 1039 cm^{-1} with the symmetric NO_2 stretching mode (ν_{sym} NO_2);[9] the ν_{sym} and ν_{as} of the NO_2 stretch thus have significant Raman intensity and exhibit similar pressure shift, but the latter is much stronger in IR (Fig. 5), consistent with its expected larger dipole moment.

B. High pressure phase transition

The high pressure x-ray diffraction patterns (Fig. 6) show generally small changes with compression to 9 GPa. Compression beyond 9 GPa produces a substantial shift in the pattern, indicating the onset of a structural phase transition by 14 GPa. The new structure is referred to as phase II, and the initial structure as phase I. As is shown in Fig. 6, markedly different patterns are observed during the compression and decompression cycles at similar pressures, indicating hysteresis in the transition.

On decompression from ~15 GPa, phase II reverts to phase I, as indicated by the complete recovery of the Raman and x-ray signatures of phase I (Figs. 4 and 6–8). Since reconstruction of the original phase upon decompression is unlikely if the metastable molecules undergo reaction during the transformation to phase II, it can be concluded that the phase transition is displacive and involves only conformational changes in the molecules and modifications in the hydrogen bond network. The phase II structure is thus probably a distortion of the phase I structure. The x-ray diffraction patterns of phase II are consistent with a triclinic structure (Fig. 6) having slightly different unit cell parameters (Fig. 7) and slightly higher density (Fig. 8) than phase I at similar pressures, and we assume this structure in our analysis. At 8.3 GPa, the density of phase II is 1.5% greater than phase I, based on this assumption. The presence of the volume discontinuity and hysteretic effects indicate that the transition is of the first order.

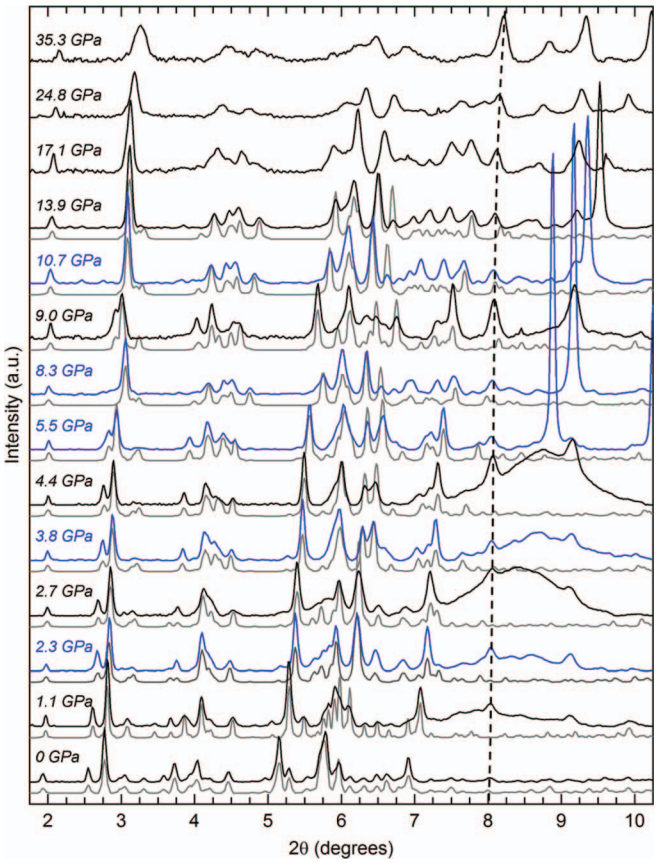

FIG. 6. X-ray diffraction data under pressure. The curves in black (blue) are diffraction patterns on compression (decompression from 13.9 GPa). The grey curves are the predicted patterns based on a unit cell refinement to observed peak locations; le Bail fit improvements not included. Black dashed line is the location of the first nonsample peak (Rhenium from gasket); to its right are additional non-sample peaks from Rhenium, and Neon, which appears as a broad hump below 5 GPa (liquid) and a sharp line above 5 GPa (solid). The x-ray wavelength was 0.3344 A.

The structural changes observed upon compression between 9 and 14 GPa can be correlated with significant modifications in the Raman spectra, including the disappearance and emergence of several features, broadening of spectral linewidths, and frequency shifts (Figs. 5 and 9), as well as

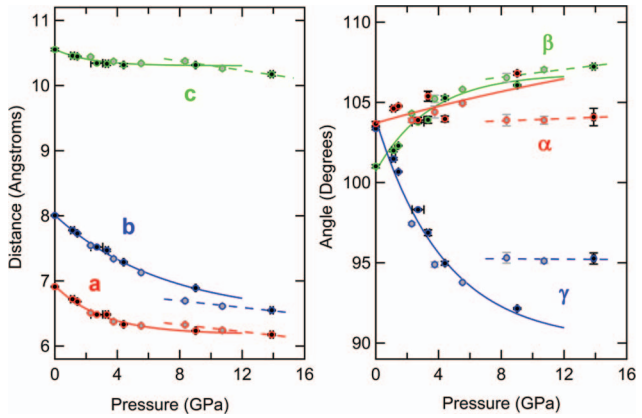

FIG. 7. Triclinic unit cell parameters for TAG-MNT under pressure. Lines are fits to the data for the low pressure (solid) and high pressure (dashed) phases. Black (grey) circles are data on compression (decompression).

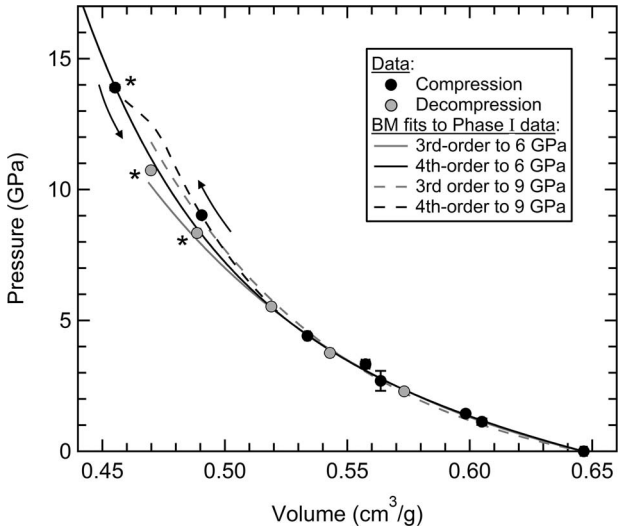

FIG. 8. Compressibility data on TAG-MNT, based on unit cell refinement using x-ray diffraction data. The black (grey) filled points were obtained upon compression (decompression). The starred points indicate data collected for phase II. The lines indicate third- and fourth-order Birch-Murnaghan fits to phase I data. Third- and fourth-order fits to 6 GPa are indistinguishable below 6 GPa, such that a third-order fit ($K_0 = 14.6$, $K^{\prime} = 4.83$) is a sufficient model; on extrapolation to higher pressure, the fourth-order fit ($K_0 = 16.2$, $K^{\prime} = 2.33$, $K^{\prime\prime} = 0.98$) provides a reasonable prediction of the high-pressure volumes in phase II, however the highest pressure datum for phase I is anomalously stiff and neither low pressure fit can predict it. For fits including the 9 GPa datum, a third-order fit shows systematic deviations from the data near 1 and 5 GPa; a fourth-order fit is necessary to represent all the data in this range. The arrows indicate the path taken by TAG-MNT upon compression (dashed black curve, based on the fourth-order fit to 9 GPa and an assumed volume collapse near 13 GPa), and upon decompression from 14 GPa (solid black curve, based on the fourth-order fit to 6 GPa).

an increase in fluorescent background. Spectral features associated with the anion $CNNO_2$ moiety exhibit particularly notable changes (Fig. 9) as discussed in more detail below. However, most Raman lines which persist through this transition lack significant discontinuities in frequency near these pressures (Figs. 5 and 10), supporting a close connection between the structures of phases I and II and an absence of chemical reactivity.

C. Continuous changes under compression at low pressure

A number of details regarding the compression behavior of TAG-MNT in phase I are worth noting. A pronounced stiffening of the equation of state beyond 6 GPa is among these (Fig. 8). Whereas a third-order BM fit to 6 GPa represents the data well to this pressure, upon extrapolation to 9 GPa the fit is in substantial disagreement with the higher pressure data; similarly, a third-order BM fit to 9 GPa is systematically offset from the data, indicating higher order terms are necessary to fit the decrease in compressibility between 6 and 9 GPa. A fourth-order BM fit to 6 GPa, when extrapolated to 9 GPa, also shows higher compressibility than the data, further highlighting the stiffening occurring above 6 GPa. Similarly, the unit cell parameters show decreased pressure sensitivity between 6 and 9 GPa (Fig. 7); for example, the *c* lattice parameter becomes constant over this pressure range. There are

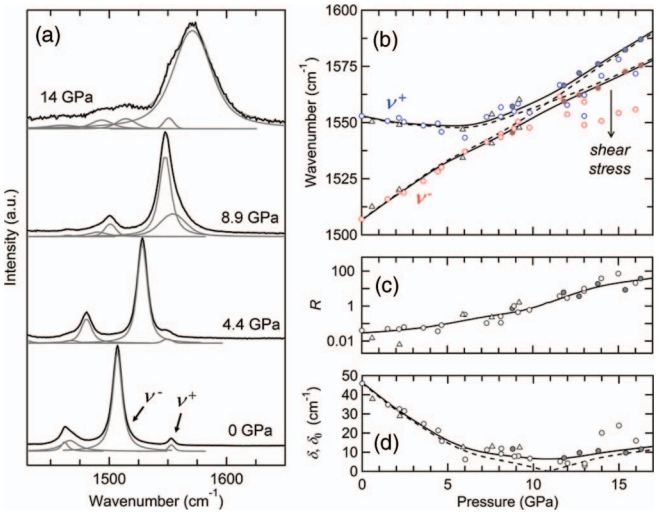

FIG. 9. Detail of interacting vibrational modes near 1500 cm^{-1} and description based on Fermi resonance theory. Both Raman and IR data are presented, shown as circles and triangles, respectively; open (filled) symbols indicate nonhydrostatic (hydrostatic) loading. (a) Raman Spectra (solid black lines) shown with fitted peaks (solid grey lines). The most intense mode (ν NO_2, 1507 cm^{-1} initial) has a frequency ν^- and intensity A^-, and the weaker, soft mode (ν C=N, 1553 cm^{-1} initial) has frequency ν^+ and intensity A^+. (b) Raman and IR frequencies, with solid (dashed) lines showing the observed (bare) frequencies in the Fermi resonance analysis. (c) Peak amplitude ratio for Raman and IR data with solid line showing the model for the Raman data. (d) Observed peak separations for Raman and IR data, with modeled actual and bare separations (solid and dashed lines, respectively). Hydrostatic loading results at high pressure were used in modeling since shear stress had a significant effect on line frequencies.

significant modifications in the behavior of Raman spectra within this "stiffening" pressure regime, including peak shifts, disappearances, and appearances (Fig. 5), substantial changes in pressure sensitivity of peaks (Figs. 5, 9, and 10), rising fluorescent background, and a pronounced mode coupling (Fig. 9) discussed below. Raman spectral lines that exhibit a decreased sensitivity to pressure between 6 and 9 GPa in turn manifest an increased sensitivity at pressures exceeding 9 GPa (Fig. 10), which correlate with the equation of state.

Raman and infrared frequencies for many vibrational features (Fig. 5) are insensitive to pressure or exhibit soft behavior under pressure (decreasing frequency upon compression). Soft modes include N–H stretching modes at high frequency, such as the ν (N–H) mode initially at 3129 cm^{-1}; the ν (C=N) mode at 1553 cm^{-1}; and several lines between 750 and 850 cm^{-1} associated with vibrations of the anion. Pressure-insensitive modes include the N–H stretching band modes (at >3100 cm^{-1}); various modes between 600 to 850 cm^{-1}; and an N–H wagging mode at 1140 cm^{-1}. It is evident that many of the moieties associated with the soft or insensitive modes are directly coupled to intermolecular hydrogen bonds (Fig. 1); indeed, such modes are often observed in hydrogen-bonded materials and are associated with the strengthening of hydrogen bonds under pressure.[27,28]

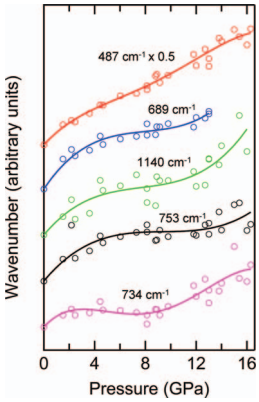

FIG. 10. Detail of selected lines in the Raman spectrum that show decreased pressure sensitivity in the stiffening regime followed by increased sensitivity at higher pressure associated with the transformation to the high-pressure phase.

The most prominent modes in the hydrogen stretch band, exhibiting relatively narrow linewidths and high intensity at low pressure, are also observed to be relatively stiff under compression, including ν (C–H) modes and the highest-frequency ν (N–H) mode (3380 cm^{-1}). These properties can be attributed to a lack of participation in hydrogen bonding for the associated moieties, as the methyl group is not expected to play a role in hydrogen bonding (Fig. 1), and at least one N–H bond appears isolated from the hydrogen bond network (N11–H11, Fig. 1). Indeed, the appearance of sharp ν (N–H) features in the nitriminotetrazolate salts[9] correlates with increasing hydrogen content in the cation, suggesting hydrogen bond saturation. The disappearance of distinct hydrogen stretching lines at high pressure can be explained by the increased participation of such initially isolated groups in hydrogen bonding.

D. Mode coupling observations

Coupling between vibration modes under pressure, such as Fermi resonances, are commonly observed in hydrogen-bonded materials due to the presence of soft modes.[27,28] In TAG-MNT, a pronounced coupling in the $CNNO_2$ group of the anion appears at about 6 GPa, as the downshifting ν (C=N) intersects the upshifting ν_{as} NO_2 (Fig. 9). At this point, the pressure variation of the peaks changes dramatically, preventing the modes from crossing, and the intensities of the peaks, initially disparate by 1–2 orders of magnitude, equalize. Such intensity exchanges and avoided crossings are features commonly associated with Fermi resonance.[27–29]

The theory of Fermi resonance[29] is used to model these observations (Fig. 9). Observed frequencies for the two interacting lines are ν^+ and ν^- with a separation δ

$$\delta = \nu^+ - \nu^-. \tag{2}$$

These have corresponding bare frequencies (natural frequencies without resonant interaction) of ν_0^+ and ν_0^- with a separation δ_0

$$\delta_0 = \nu_0^+ - \nu_0^-. \tag{3}$$

These are related via the Fermi coefficient W, which defines the coupling strength

$$\delta^2 = \delta_0^2 + 4W^2. \tag{4}$$

Bare frequencies can be calculated from observed frequencies considering that

$$(\delta - \delta_0)/2 = |\nu^+ - \nu_0^+| = |\nu^- - \nu_0^-|. \quad (5)$$

The peak intensity ratio $R = I^+/I^-$, where I^+ and I^- are the peak intensities, is given by

$$R = \left[\frac{\sqrt{\delta + \delta_0}\sqrt{R_0} + \sqrt{\delta - \delta_0}}{\sqrt{\delta - \delta_0}\sqrt{R_0} - \sqrt{\delta + \delta_0}}\right]^2, \quad (6)$$

where R_0 is the unperturbed (bare) intensity ratio (I_0^+/I_0^-) which is finite in the case of two interacting fundamentals.

At the crossover of the bare frequencies (i.e., where $\delta_0 = 0$), $\delta = 2W$; from the data we estimate $W \approx 6 \pm 1$ cm^{-1} near the crossover (Fig. 9(d)). The observed ambient pressure intensity ratio (~0.04 for Raman peaks) can be used to estimate R_0. We take W and R_0 to be constants, and optimize them for the best fit to the observed data (Fig. 9), giving $W = 3.2$ and $R_0 = 0.01$. The good reproduction of the data using this simple model, particularly the observed evolution of R (Fig. 9(c)), provides strong evidence that Fermi resonance is occurring.

The interaction between these fundamental vibrations reinforces their identification with adjacent moieties of the same molecule. A similar resonance may occur under pressure in C–H stretch modes associated with the methyl group (3012 and 3032 cm^{-1} initially). This behavior contrasts with other clear cases of frequency crossing upon compression at 1150 and 1470 cm^{-1} which show no evidence for mode interaction. These exhibit a distinct crossover point defined by overlap of peaks such that only fitting a single peak can be justified. In at least the former case, the absence of interaction can be explained by mode assignment to different molecules (Table II).

E. Pressure-induced polymerization

Similarities between pristine TAG-MNT and that recovered from compression to 15 GPa (Figs. 4 and 6–8) provide strong evidence that significant chemistry does not accompany the transition between phases I and II. However, when TAG-MNT is compressed beyond 15 GPa, concomitant changes in the x-ray diffraction and Raman spectroscopic data suggest the onset of pressure-induced chemistry, polymerization, and amorphization.

As shown in Fig. 6, the x-ray diffraction peaks both broadened and weakened in intensity between 13 and 35 GPa, with the intensity of the weak lines approaching the noise level. At and above 17 GPa, attempts to model the diffraction pattern based on a triclinic structure were unsuccessful, with all refinement attempts resulting in poor convergence between the predicted and experimental patterns and anomalously low densities. Moreover, the peak broadening suggests a gradual loss of long range order. However, we find that distinct diffraction peaks are visible to 35 GPa (Fig. 6), indicating that the material remains at least semi-crystalline to this pressure.

Concurrently, the *in situ* Raman spectroscopic data collected within this pressure regime show a generalized broadening and loss of lines, coupled with high background and high photochemical sensitivity. Nonhydrostatic compression to 60 GPa led to a near-total loss of *in situ* Raman signal, a few broad Raman bands, and a high background (Fig. 5); the loss of distinct Raman features, and appearance of a few broad Raman bands in this regime can be attributed to a disordered bond network in a material that has been completely polymerized. To further investigate chemical changes induced by pressure beyond 15 GPa, where samples exhibited high *in situ* photochemical sensitivity and high background signal at preferred Raman laser wavelengths, samples were compressed to the desired pressure and decompressed (Figs. 4 and 11), on the premise that pressure-induced reactions would not be reversible.

Compression to 25 GPa and complete decompression produced a polycrystalline powder and a fluid. The powder, initially colorless, became brown-red on exposure to air; Raman spectra of the powder plus fluid exhibited all the expected lines of pristine TAG-MNT in addition to new spectral signatures (Fig. 4), indicating that the sample had partially reacted but that a large fraction of pure TAG-MNT remained. The fluid, where it could be observed independently of the powder, exhibited a few strong lines originally associated with the anion (i.e., NO_2 and C–H modes), but lacked strong lines originally associated with the cation (i.e., N–H modes). Compression to 60 GPa and complete decompression produced a pasty fluid substance and gaseous products. Decompression products were further studied *in situ* at a low pressure (2–3 GPa) to characterize reaction products without phase separation, loss, or reaction with air (Fig. 11).

For decompression from 25 GPa to ~3 GPa, a few differences can be seen in the decompressed samples compared to a sample only compressed to 3 GPa (Fig. 11). Most notably, lines associated with the $CNNO_2$ moiety (i.e., the coupled modes near 1500 cm^{-1}) have shifted. This is evidence that the anion remains largely unchanged, but the local environment of the $CNNO_2$ group has been altered. This effect was found to occur identically for hydrostatic and

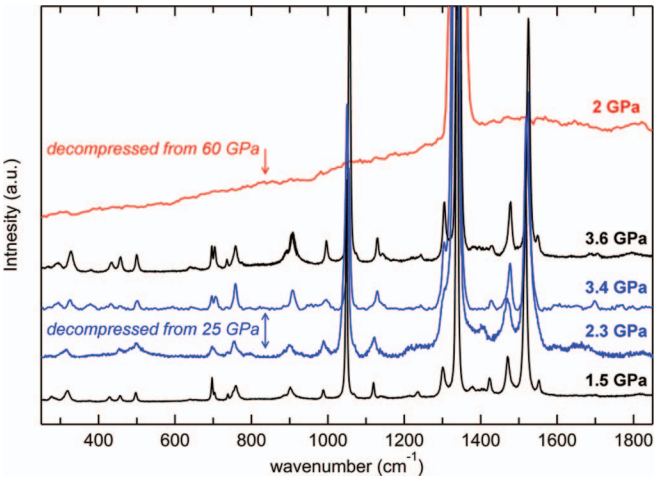

FIG. 11. Comparison of Raman measurements taken on compression (black) with those obtained on decompression. Data from samples decompressed from 25 GPa and 60 GPa are blue and red, respectively; blue curves correspond to samples loaded hydrostatically (upper) and nonhydrostatically (lower). Excitation wavelengths from top to bottom are 488, 488, 632, 457, and 488 nm.

nonhydrostatic loading (Fig. 11). For nonhydrostatic compression to 60 GPa and decompression to ∼2 GPa, the recovered sample exhibited a substantial background and no distinct Raman signals (Fig. 11), indicating a total, irreversible polymerization of the material; this corroborates the Raman observations at high pressure, which show similar spectra.

These results show that between 15 and 25 GPa, partial chemical decomposition of TAG-MNT is coupled with a loss of long range structural order. Chemistry (and amorphization) thus occurs heterogeneously. With increasing pressure TAG-MNT is consumed by a total reconstructive transition to a polymeric state.

F. Effect of shear stress

In diamond anvil cells loaded without pressure media, or in hydrostatically loaded cells where the sample cavity had closed down on the sample under pressure, clear effects of shear stress are observed. X-ray diffraction patterns were significantly degraded and, when no pressure medium was used, bore no similarity to the corresponding patterns of TAG-MNT collected under hydrostatic conditions. Peak broadening due to pressure gradients could not explain the changes in pattern appearance.

The Raman features of TAG-MNT were identical in hydrostatic and nonhydrostatic loading to 17 GPa (Figs. 5 and 9), with the exception of the NO_2 (1507 cm^{-1}) and C=N (1553 cm^{-1}) stretching modes. Compared to hydrostatic loading, a systematic shift of these two modes to lower frequencies is observed in nonhydrostatic loading. This trend indicates that shear stress affects bond energies of the anion $CNNO_2$ moiety, a long, isolated molecular unit that extends out from the molecular core, which likely contributes to its shear stress sensitivity. Because the Raman spectra rule out major chemistry occurring due to shear stress, the substantial deviation of nonhydrostatic diffraction patterns from hydrostatic ones is most likely the result of preferred orientation, a conclusion which is reinforced by nonuniform angular intensity observed in nonhydrostatic diffraction images. Thus, our results indicate shear stress predominantly influences the long range order of TAG-MNT, and more subtly influences molecular properties.

G. Photochemistry

At high powers of 457 and 488 nm laser excitation, sample degradation was observed in the Raman spectrum due to photochemically induced reactions (Fig. 12), principally evidenced by formation of a broad peak centered at 2344 cm^{-1} that we attribute to the formation of molecular nitrogen (N_2 vibron) based on the strong intensity of this line and its similarity in frequency to that of molecular nitrogen.[30] In contrast to the vibronic behavior of pure nitrogen,[30] which exhibits multiple Raman features that shift strongly as a function of pressure, the single vibronic peak observed in the spectrum of TAG-MNT exhibited no discernible shift with pressure. This trend is consistent with N_2 existing as isolated molecules or clusters trapped (likely with other decomposition products)

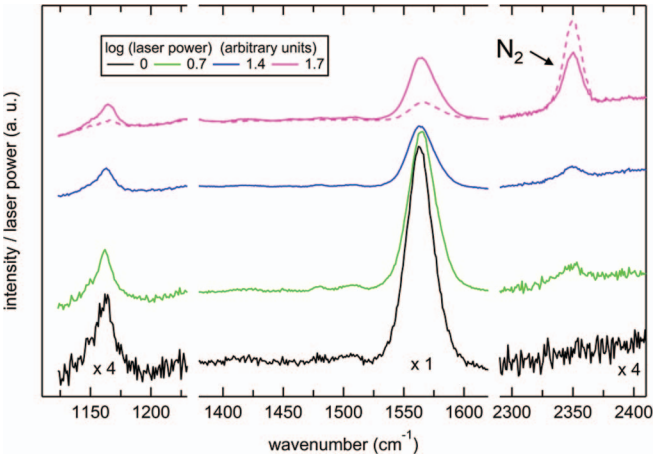

FIG. 12. Raman measurements of photochemical transformation of TAG-MNT compressed to 12.2 GPa, with excitation from a 457 nm laser. Spectral intensity is normalized to laser power and shifted arbitrarily in the y-axis. Data correspond to 5 min of accumulation, beginning either with laser shut-on (solid) or ∼15 min after laser shut-on (dashed). For each power level a fresh area of sample was studied. The transformation was accompanied by the appearance of discolored spots in the sample, which grew in size with increasing power and time. Small variations (several cm^{-1}) in Raman line positions (i.e., of the strong line at 1565 cm^{-1}) were not systematically related to laser power, and are attributed to pressure gradients in the nonhydrostatic sample. Most Raman measurements reported in this study were made using excitation of 488 nm, for which photochemical effects were less pronounced.

in a matrix of untransformed TAG-MNT. The onset of photochemical reactions is principally observed in the Raman spectrum above 7 GPa, and becomes very pronounced above 13 GPa (in Phase II); however, in some cases it was observed even in a single crystal at room pressure. It is noted that photochemical production of molecular nitrogen also occurred in the polymeric phase.

Higher laser powers and 457 and 488 nm excitation also resulted in degraded Raman spectra over time, and caused visible sample damage at pressures above 12 GPa. As the intensity of the N_2 vibronic feature increased, the intensity of other Raman features decreased and there was a significant rise in the background signal. Particular sensitivity to photochemical damage was observed in the N–H stretching bands above 3100 cm^{-1} in the Raman spectra, consistent with the destruction of N–H functional groups in the formation of N_2. However, no systematic changes in Raman line positions were observed as a consequence of photochemical transformation. Generally, photochemical reactions could be avoided with reduced laser power and longer collection times, and longer wavelength Raman excitation (i.e., 632 nm).

V. DISCUSSION

The observations of the lattice constants and volume of TAG-MNT under pressure suggest that degrees of freedom for the deformation of phase I are reduced above 6 GPa, leading to a sharp stiffening of the unit cell. Modifications in vibrational spectra at and above 6 GPa show that changes in molecular state accompany this stiffening. Most prominently, the onset of visible exchange in vibrational character between fundamental NO_2 and C=N vibration modes in the $CNNO_2$

moiety of the anion occurs with this stiffening, as does a dramatic shift in pressure dependence of the C=N mode's bare frequency. The vanishing of this exchange, wherein the weaker line (character of ν C=N) has clearly shifted to the other side of the strong line (character of ν NO_2), corresponds with the high-pressure transformation to phase II and the concomitant softening of the equation of state. This indicates a correlation between mode coupling and the detailed compression behavior of TAG-MNT.

Given that the coupled modes correspond to the hanging $CNNO_2$ moiety, which extends from the tetrazole core of the anion and is likely to be strongly deformed under compression, it is possible that mode coupling in this moiety under pressure is connected with the response of the molecule and bulk to compression. The $CNNO_2$ moeity is roughly a chain (C=N–N) orientated parallel to the *c* crystallographic axis (Fig. 1); since the most compressible orientation of this moiety is likely along the chain (via a change in C=N–N bond angle), the freezing of the *c*-axis in the regime of visible coupling (Fig. 7) is consistent with a restriction on deformation of the $CNNO_2$ moeity occurring simultaneously with coupling effects. Also, the strengthening of hydrogen bonding with the C=N–N chain, manifested below 6 GPa as a softening and rapid broadening of the ν C=N vibrational mode, is limited above 6 GPa as this mode stiffens concomitantly with the onset of visible coupling; plausibly, as the soft mode adopts some character of the stiff mode, strengthening of hydrogen bonding with this moiety is resisted, thereby influencing conformation and compressibility.

The self-consistent description of the coupled modes with Fermi resonance theory suggests that the observations are indeed an example of Fermi resonance, in which two fundamental modes, not strongly interacting at room pressure, interact strongly at pressure. The apparent interaction between resonance and system compressibility would be anomalous, however, as we know of no other system in which this effect has been identified; indeed, for materials familiar to the present authors, Fermi resonance is known to occur passively under pressure, responding to but not controlling bulk compression. Indeed, we may be observing a passive resonance effect aligned with anomalies in compressibility in TAG-MNT. On the other hand, steric controls on compression should be particularly important for this chemically complex substance, compared to materials with simpler molecular constituents, and so molecular energy redistribution by resonance may yield more visible effects on compressibility than are typically encountered. Also, the present coupling involves skeletal mode fundamentals, rather than overtones and hydrogen deformation modes typically observed in Fermi resonances, which could lead to differences from other studies and more first-order effects on bulk properties. Another anomalous feature of the present system is the sharp change in the pressure dependence of the bare frequency for the soft mode ν^+ (Fig. 9) coincident with the onset of visible coupling, which is consistent with resonance having a direct effect on the compression response.

Consistent with this picture, a main mechanism of compression in TAG-MNT could be the deformation of the $CNNO_2$ moiety and the strengthening of hydrogen bonding with the C–N–N "elbow" of this moiety. Limitations on these processes imposed by the coupling of the ν C=N and ν NO_2 modes could then result in a stiffening of the equation of state as these modes begin to exchange character under pressure. Upon further loading, a phase transition—corresponding to a reduction in character exchange—accommodates further compression. Given that the volumetric shift due to the transition is comparable in magnitude, but opposite in sign, to that associated with stiffening prior to the transition ($\sim$1% in volume, Fig. 9), it is possible the phase transition corresponds to a sudden relaxation of constraints imposed by resonance. To further evaluate whether Fermi resonance has an active effect on compression or responds passively to it, studies on other nitriminotetrazolate salts might be illuminating, as the $CNNO_2$ mode coupling should be general to this class of materials.

At higher pressure, chemical decomposition and polymerization are necessary to open further degrees of freedom for compression. The cause of decomposition is likely related to the lack of available molecular packing configurations for these large and highly asymmetric molecules, that is, conformational changes are no longer sufficient to accommodate the closing distance between molecules. The strengthening of hydrogen bonding may also play an important role in the transition to the polymeric, disordered state, as is the case for formic acid,[27] by enabling intramolecular decomposition or intermolecular covalent bonding. At the pressures where polymerization occurs, hydrogen bonding is likely to become more covalent in nature, effectively initiating the polymerization reaction.

VI. CONCLUSIONS

The behavior of TAG-MNT under pressure can be best broken into four stages: (1) a region of normal compressibility to pressures near 6 GPa, associated with the strengthening of hydrogen bonds; (2) the onset of anomalous stiffening at $\sim$6 GPa, possibly resulting from vibrational mode coupling (Fermi resonance) in the anion; (3) a displacive phase transition near 13 GPa to a denser crystalline phase (phase II); and (4) a continuous reconstructive transition at pressures exceeding $\sim$20 GPa that ultimately leads to the formation of a polymeric, disordered state. Both the transition to phase II and pressure-induced reaction occur at conditions directly relevant to detonation of TAG-MNT.[9]

The high pressure structure (phase II) is found here to be reasonably described as a distortion of the initial structure (phase I), where anion and cation retain their bonding character but undergo a (reversible) change in conformity coincident with a displacive structural transition. Thus, the phase transition is not decomposition, rather it is to another state of TAG-MNT. Phase II is reasonably described as a unique phase of TAG-MNT, though unit cell parameters and Raman features are similar to phase I. Both phases are observed at the same pressure with distinctly different diffraction patterns, due to hysteresis (Fig. 6). Phase II also exhibits substantial differences from phase I in terms of its enhanced chemical sensitivity to shear stress (Figs. 5 and 9) and radiation.

The most interesting spectroscopic band of TAG-MNT observed in this study is comprised of C=N and NO_2 stretch modes (1500–1600 cm^{-1}) associated with the $CNNO_2$ moiety of nitriminotetrazole. These are active in both IR and Raman, and are highly sensitive to and diagnostic of the molecular environment. At ambient pressure, their frequencies shift considerably when the molecule is placed in salt.[9] At high pressure, shear stresses and partial chemical decomposition produce frequency shifts in these modes, relative to frequencies seen in hydrostatically compressed, pure TAG-MNT. Additionally, they exhibit a pronounced mode coupling under pressure which plausibly influences bulk compression behavior and the equation of state. Thus, properties of this band strongly correlate with the physical and chemical state of TAG-MNT. The phenomena associated with this band will likely appear in other nitriminotetrazole-based materials. For example, Fermi resonance in this band seemingly influences the ambient-pressure vibrational properties of these materials: for pure nitriminotetrazole, the C=N and NO_2 stretching modes are close in frequency and exhibit comparable intensities, whereas in the salts the modes are more disparate in frequency, with one mode exhibiting dramatically reduced intensity.[9]

ACKNOWLEDGMENTS

The authors would like to thank M. Somayazulu for experimental assistance, Vitali Prakapenka and the GSECARS staff for help in conducting synchrotron experiments, and two anonymous reviewers for comments on this manuscript. E. F. C. Byrd is thanked for his assistance in performing the quantum chemical calculations on TAG-MNT. This work was supported by the US Army Research Office (ARO-56122-CH-H), the US Army Research Office High School Apprenticeship Program (ARO-HSAP), and the Department of Energy National Nuclear Security Administration (Carnegie/DOE Alliance Center; DE-FC52-08NA28554). GSECARS is supported by the National Science Foundation – Earth Sciences (EAR-0622171) and Department of Energy – Geosciences (DE-FG02-94ER14466). Use of the Advanced Photon Source was supported by the U.S. Department of Energy, Office of Science, Office of Basic Energy Sciences, under Contract No. DE-AC02-06CH11357. Infrared measurements were performed at the U2A beamline at the NSLS of BNL (DOE Contract No. DE-AC02-98CH10886). The U2A beamline is supported by COMPRES, the Consortium for Materials Properties Research in Earth Sciences, under NSF Cooperative Agreement Grant No. EAR-0135554 and the U.S. DOE (CDAC, Contract No. DE-FC03-03N00144).

[1] H. H. Cady and L. C. Smith, Los Alamos Technical Report no. LAMS-2652, 1962.
[2] S. M. Peiris and T. P. Russell, J. Phys. Chem. A **107**(6), 944 (2003).
[3] M. I. Eremets, I. A. Trojan, A. G. Gavriliuk, and S. A. Medvedev, in *Static Compression of Energetic Materials*, edited by S. M. Peiris and G. J. Piermarini (Springer-Verlag Berlin Heidelberg, Heidelberg, 2008), p. 75.
[4] M. I. Eremets, R. J. Hemley, H. K. Mao, and E. Gregoryanz, Nature (London) **411**(6834), 170 (2001).
[5] A. F. Goncharov, E. Gregoryanz, H. K. Mao, Z. Liu, and R. J. Hemley, Phys. Rev. Lett. **85**(6), 1262 (2000).
[6] M. I. Eremets, A. G. Gavriliuk, I. A. Trojan, D. A. Dzivenko, and R. Boehler, Nat. Mater. **3**(8), 558 (2004).
[7] E. Gregoryanz, A. F. Goncharov, C. Sanloup, M. Somayazulu, H. K. Mao, and R. J. Hemley, J. Chem. Phys. **126**(18), 5 (2007).
[8] M. J. Lipp, J. P. Klepeis, B. J. Baer, H. Cynn, W. J. Evans, V. Iota, and C. S. Yoo, Phys. Rev. B **76**(1), 014113 (2007).
[9] T. M. Klapötke, J. Stierstorfer, and A. U. Wallek, Chem. Mater. **20**(13), 4519 (2008).
[10] J. A. Ciezak, Propellants, Explos., Pyrotech. **35**(4), 373 (2010).
[11] T. M. Klapötke, *New Nitrogen-Rich High Explosives, in High-Energy Density Materials* (Springer-Verlag, Berlin, 2007).
[12] C. S. Yoo and H. Cynn, J. Chem. Phys. **111**(22), 10229 (1999).
[13] J. J. Dick, J. Phys. Chem. **97**(23), 6193 (1993).
[14] H. K. Mao, J. Xu, and P. M. Bell, J. Geophys. Res. [Solid Earth Planets] **91**(B5), 4673 (1986).
[15] A. F. Goncharov, V. V. Struzhkin, R. J. Hemley, H. K. Mao, and Z. Liu, in *Science and Technology of High Pressure: Proceedings of AIRAPT-17*, edited by M. H. Manghnani, W. J. Nellis, and M. F. Nicol (Universities Press, Hyderabad, India, 2000), p. 90.
[16] Z. Liu, J. Hu, H. Yang, H. K. Mao, and R. J. Hemley, J. Phys. Condens. Matter **14**(44), 10641 (2002).
[17] V. B. Prakapenka, A. Kubo, A. Kuznetsov, A. Laskin, O. Shkurikhin, P. Dera, M. L. Rivers, and S. R. Sutton, High Pressure Res. **28**(3), 225 (2008).
[18] A. P. Hammersley, S. O. Svensson, M. Hanfland, A. N. Fitch, and D. Hausermann, High Pressure Res. **14**(4–6), 235 (1996).
[19] O. Tschauner, B. Kiefer, Y. Lee, M. Pravica, M. Nicol, and E. Kim, J. Chem. Phys. **127**(9), 094502 (2007).
[20] F. Birch, J. Geophys. Res. **83**(NB3), 1257, doi:10.1029/JB083iB03p01257 (1978).
[21] M. J. Frisch, G. W. Trucks, H. B. Schlegel *et al.*, GAUSSIAN 98, Revision A7, Gaussian, Inc., Pittsburgh, PA, 2001.
[22] A. D. Becke, J. Chem. Phys. **98**(7), 5648 (1993).
[23] C. T. Lee, W. T. Yang, and R. G. Parr, Phys. Rev. B **37**(2), 785 (1988).
[24] S. H. Vosko, L. Wilk, and M. Nusair, Can. J. Phys. **58**(8), 1200 (1980).
[25] See http://cccbdb.nist.gov/vibscalejust.asp for precomputed vibrational scaling factors.
[26] H. H. Cady, J. Chem. Eng. Data **17**(3), 369 (1972).
[27] A. F. Goncharov, M. R. Manaa, J. M. Zaug, R. H. Gee, L. E. Fried, and W. B. Montgomery, Phys. Rev. Lett. **94**(6), 065505 (2005).
[28] V. V. Struzhkin, A. F. Goncharov, R. J. Hemley, and H.-k. Mao, Phys. Rev. Lett. **78**(23), 4446 (1997).
[29] J. F. Bertran, L. Ballester, L. Dobrihalova, N. Sanchez, and R. Arrieta, Spectrochim. Acta, Part A **24**(11), 1765 (1968).
[30] R. Lesar, S. A. Ekberg, L. H. Jones, R. L. Mills, L. A. Schwalbe, and D. Schiferl, Solid State Commun. **32**(2), 131 (1979).